vehicles

MDPI

Article

Seventh-Degree Polynomial-Based Single Lane Change Trajectory Planning and Four-Wheel Steering Model Predictive Tracking Control for Intelligent Vehicles

Fei Lai [1,2,*] and Chaoqun Huang [3]

[1] School of Vehicle Engineering, Chongqing University of Technology, Chongqing 400054, China
[2] Key Laboratory of Advanced Manufacturing Technology for Automobile Parts, Ministry of Education, Chongqing 400054, China
[3] Institute of Intelligent Manufacturing and Automotive, Chongqing Technology and Business Institute, Chongqing 401520, China; huangchaoqun@cqtbi.edu.cn
* Correspondence: laifeichq@cqut.edu.cn

Abstract: Single lane changing is one of the typical scenarios in vehicle driving. Planning a suitable single lane changing trajectory and tracking that trajectory accurately is very important for intelligent vehicles. The contribution of this study is twofold: (i) to plan lane change trajectories that cater to different driving styles (including aspects such as safety, efficiency, comfort, and balanced performance) by a 7th-degree polynomial; and (ii) to track the predefined trajectory by model predictive control (MPC) through four-wheel steering. The growing complexity of autonomous driving systems requires precise and comfortable trajectory planning and tracking. While 5th-degree polynomials are commonly used for single-lane change maneuvers, they may fail to adequately address lateral jerk, resulting in less comfortable trajectories. The main challenges are: (i) trajectory planning and (ii) trajectory tracking. Front-wheel steering MPC, although widely used, struggles to accurately track trajectories from point mass models, especially when considering vehicle dynamics, leading to excessive lateral jerk. To address these issues, we propose a novel approach combining: (i) 7th-degree polynomial trajectory planning, which provides better control over lateral jerk for smoother and more comfortable maneuvers, and (ii) four-wheel steering MPC, which offers superior maneuverability and control compared to front-wheel steering, allowing for more precise trajectory tracking. Extensive MATLAB/Simulink simulations demonstrate the effectiveness of our approach, showing improved comfort and tracking performance. Key findings include: (i) improved trajectory tracking: Four-wheel steering MPC outperforms front-wheel steering in accurately following desired trajectories, especially when considering vehicle dynamics. (ii) better ride comfort: 7th-degree polynomial trajectories, with improved control over lateral jerk, result in a smoother driving experience. Combining these two techniques enables safer, more efficient, and more comfortable autonomous driving.

Keywords: intelligent vehicle; single lane change; trajectory planning; model predictive control; four-wheel steering; 7th-degree polynomial

Citation: Lai, F.; Huang, C. Seventh-Degree Polynomial-Based Single Lane Change Trajectory Planning and Four-Wheel Steering Model Predictive Tracking Control for Intelligent Vehicles. *Vehicles* **2024**, *6*, 2228–2250. https://doi.org/10.3390/vehicles6040109

Academic Editor: Chao Huang

Received: 3 November 2024
Revised: 11 December 2024
Accepted: 20 December 2024
Published: 23 December 2024

1. Introduction

1.1. Motivations

Lane change maneuvers, such as overtaking or avoiding obstacles, are common driving scenarios for intelligent vehicles, typically involving a single lane change. Lane change trajectories greatly affect safety, efficiency, and comfort. Furthermore, even with the same lane change trajectory, varying tracking control methods can yield different control outcomes.

1.2. State-of-the-Art

There are three primary reasons for a vehicle to change lanes: (i) a breakdown ahead, (ii) overtaking, and (iii) traffic regulations. Research on single lane changes has concentrated on both trajectory planning and tracking. Most trajectory planning approaches simplify the vehicle as a point mass model, neglecting its dynamics. Optimal distance and time for lane changes can be determined using 5th-degree polynomial trajectory planning for high initial velocities [1]. In a sudden lane change situation, the clearance curve derived from the bicycle model is closely related to the point mass model [2]. By means of Pontryagin's maximum principle, an appropriate choice of Lagrangian functions can produce almost time-optimal continuous curvature paths [3]. Arcs, polynomials, sinusoidal slopes, trapezoids and trapezoidal acceleration curves can be used for emergency lane change path planning [4]. Neural networks can predict self-vehicle and neighboring vehicle trajectories to prevent collisions [5]. A framework for generating and displaying 5th-degree polynomial curves as self-driving car trajectories was proposed in [6]. Overtaking lane change trajectories have also been investigated [7–10]. Based on the optimal prediction method, ref. [7] designed a smooth and safe optimal trajectory generation scheme for overtaking self-driving vehicles, which can be used in various traffic scenarios. Viewing trajectory planning as an optimization task, a control design method with strong robustness was presented in [8]. A two-stage path planning strategy has also been introduced [9], where the first step considered vehicle dynamic behavior and road boundary conditions for offline optimization, and the second stage considered dynamic obstacles to generate continuous paths in real time. By combining Bessel curves with model predictive control (MPC), ref. [10] proposed a hybrid planning method to solve the collision avoidance and overtaking problems. Model predictive control algorithms have been used to plan vehicle trajectories [11–13]. Using 5th-degree polynomials, a lane changing trajectory considering comfort and efficiency was proposed [14]. Cooperative collision avoidance trajectories were investigated by Telematics [15,16]. Deep learning [17], scene understanding and motion prediction [18] have all been used to plan vehicle motion trajectories. A trajectory planning method considering feasibility, safety and passenger acceptance was proposed in [19,20] and presented new motion primitives for autonomous racing to efficiently approximate minimum-time trajectories. Ref. [21] introduced a high-speed, two-stage, multi-layer graph-based trajectory planner capable of reaching speeds of up to 212 km/h.

Trajectory tracking is the second priority for single lane changes, following trajectory planning. It typically involves either purely lateral control, without accounting for longitudinal velocity changes, or a simultaneous consideration of both longitudinal and lateral motions. However, few studies focus solely on longitudinal trajectory tracking. A full suite of performance indicators encompassing precision, robustness, and user experience was proposed for a comprehensive assessment of lateral control [22]. Data-driven modeling approaches have also been used for lateral vehicle maneuvering control with uncertain model parameters [23]. As far as control methods are concerned, trajectory tracking control broadly consists of pure tracking control by vehicle geometric models [24], Stanley tracking control by geometric models [25], model predictive control by kinematic models [26], optimal control by vehicle dynamic models [27–30], and model predictive control by dynamic models [31–34]. In addition to these, sliding mode control [35] and fuzzy control [36] have also been used for trajectory tracking. A novel state feedback control method considering real-time changes in model parameters was proposed in [37]. A unified control architecture for enhancing vehicle stability and path following was developed, that took into account longitudinal and lateral slip in tire dynamics [38]. Based on the consideration of longitudinal–lateral coupling effects in vehicle dynamics, ref. [39] used a backward-looking strategy to track the trajectory. A trajectory tracking control method combining deep learning and a rapidly-exploring random tree (RRT) was proposed in [40]. Classical, geometric and predictive control trajectory tracking control methods have been compared, and three different types of trajectory tracking tests were realized on an experimental prototype [41]. A nonlinear adaptive fractional-order terminal sliding mode control scheme was proposed

to ensure robust path tracking performance of self-driving vehicles with uncertain dynamics [42]. A novel pole-seeking controller for trajectory tracking of all-wheel-drive quadricycles was presented in [43]. Currently, research on four-wheel steering systems mainly focuses on the following three areas: (1) Control algorithms, including research on model-based [44] and model-free control approaches [45]; (2) Integrated control, including integration with braking and suspension systems to enhance vehicle performance at the limit [46], as well as integration with surrounding environmental information to improve collision avoidance and active safety in autonomous vehicles [47]; (3) Fully independent four-wheel steering, aimed at enhancing vehicle maneuverability and active safety [48,49]. However, research on using four-wheel steering to track different reference trajectories is relatively limited. To summarize, the use of 5th-degree polynomials for trajectory planning may lead to less comfortable driving experiences, as they may not effectively address lateral jerk constraints. Furthermore, despite the widespread application of front-wheel steering MPC, it can struggle to accurately follow trajectories derived from simplified point mass vehicle models, especially when actual vehicle dynamics are taken into account. This discrepancy can manifest as excessive lateral acceleration changes, compromising ride comfort and vehicle stability.

1.3. Contributions

This study makes a novel contribution by proposing a lane-changing trajectory that satisfies various driving styles. This trajectory ensures that the vehicle achieves optimal performance in a specific aspect or the best overall performance during the lane-changing process, depending on different driving styles. Furthermore, a model predictive control approach is utilized to achieve accurate path tracking with both front- and rear-wheel steering actuators. Compared to front-wheel steering MPC, four-wheel steering MPC provides better overall tracking performance.

1.4. Structure Overview

The organizational structure of this study is as follows: Section 1 serves as the introduction. Section 2 explains the control objectives. Section 3 provides a detailed description of the proposed control method, encompassing trajectory planning and tracking control algorithms. Section 4 is a comparison of the simulation results. Section 5 concludes this study.

2. Issues to Be Addressed

In this study, we mainly address the trajectory planning and trajectory tracking problems during single lane maneuvering of intelligent vehicles, as depicted in Figure 1. When the subject vehicle encounters a fixed vehicle or a vehicle moving slowly in the same lane, there are three key factors involved in how to avoid the front vehicle: (i) when to change lanes, i.e., how far away from the front vehicle to start the steering maneuver; (ii) how to change lanes, i.e., how to design the vehicle's trajectory during a lane change; and (iii) what kind of control strategy is employed to follow the desired trajectory. Different trajectory planning algorithms produce different lane changing trajectories. Even for the same planning algorithm, under different constraints, there are significant differences in the planned trajectories. For example, when the maximum lateral acceleration constraint is given during the lane change, the planned trajectories are different from the trajectories under the maximum jerk constraint. In addition, even for the same lane-changing trajectory, if different tracking control methods are used, the resulting tracking control effects are also different. In order to simplify the study, it assumes that the vehicle longitudinal speed remains constant at both the start and end of the lane change.

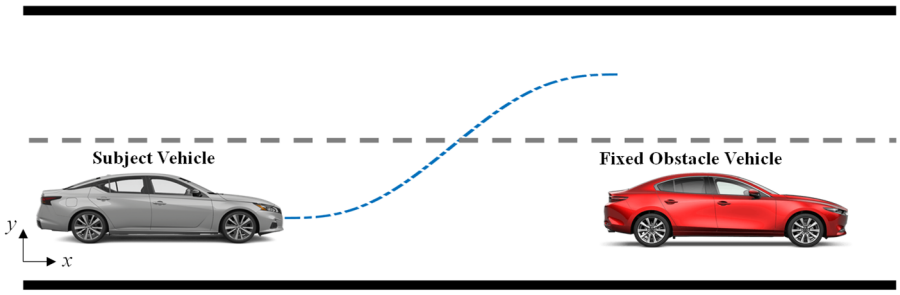

Figure 1. Single lane change maneuver.

3. Control System Synthesis

The test diagram of proposed method in this study is shown in Figure 2, which is composed of four main components: (i) environment perception module; (ii) path planning module; (iii) trajectory tracking control module; and (iv) vehicle modeling module. Among these, the environment perception information is obtained from the vehicle sensors and fusion algorithm, which is assumed in this study to be known beforehand. Vehicle routing can use either a 5th degree polynomial or a 7th-degree polynomial. The 7th-degree polynomial plans a smoother path than the 5th-degree polynomial, due to the consideration of the jerk (the derivative of the acceleration) constraint. Trajectory tracking is performed using a model predictive control method to track the preplanned trajectory by two control strategies, i.e., front-wheel steering or four-wheel steering. The performance of the proposed control algorithm is verified using a two degree of freedom (DOF) single track model of the vehicle dynamics.

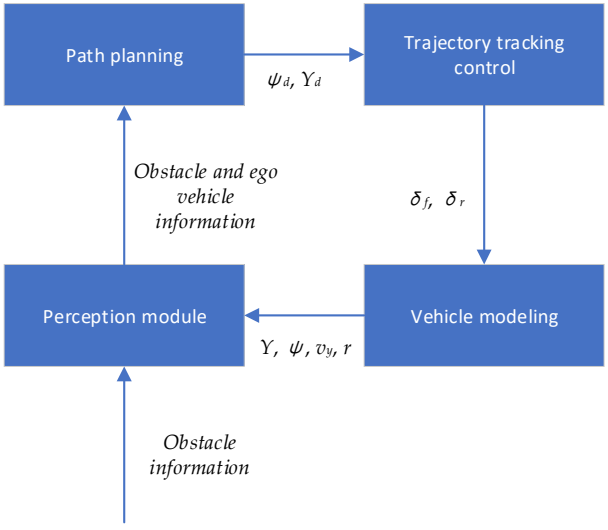

Figure 2. Test diagram of the proposed method.

3.1. Path Planning

Research on lane change trajectory often adopts quintic polynomials. In general, cubic polynomials are suitable for determining the vehicle's velocity and position, whereas quintic polynomials can additionally determine acceleration. To ensure smooth lane changes, this study conducts trajectory planning using a 7th-degree polynomial, which can determine the vehicle's displacement, speed, acceleration, and jerk.

The expressions for quintic polynomial and 7th-degree polynomial are shown as follows:

$$\begin{cases} x(t) = p_5t^5 + p_4t^4 + p_3t^3 + p_2t^2 + p_1t + p_0 \\ y(t) = q_5t^5 + q_4t^4 + q_3t^3 + q_2t^2 + q_1t + q_0 \end{cases} \quad (1)$$

$$\begin{cases} x(t) = m_7t^7 + m_6t^6 + m_5t^5 + m_4t^4 + m_3t^3 + m_2t^2 + m_1t + m_0 \\ y(t) = n_7t^7 + n_6t^6 + n_5t^5 + n_4t^4 + n_3t^3 + n_2t^2 + n_1t + n_0 \end{cases} \tag{2}$$

Here, t represents time, x denotes longitudinal displacement, y stands for lateral displacement, and a_0–a_3, b_0–b_3, p_0–p_5, q_0–q_5, m_0–m_7, and n_0–n_7 are the polynomial fitting coefficients. The boundary conditions for the quintic polynomial that must be satisfied for vehicle lane changing are as follows:

$$\begin{cases} x(t_s) = 0, \dot{x}(t_s) = v_1, \ddot{x}(t_s) = 0, x\left(t_f\right) = L, \dot{x}\left(t_f\right) = v_2, \ddot{x}\left(t_f\right) = 0 \\ y(t_s) = 0, \dot{y}(t_s) = 0, \ddot{y}(t_s) = 0, y\left(t_f\right) = W, \dot{y}\left(t_f\right) = 0, \ddot{y}\left(t_f\right) = 0 \end{cases} \tag{3}$$

where t_s is the starting time of the lane change, t_f is the ending time of the lane change, v_1 is the starting forward speed when changing lanes, v_2 is the final longitudinal velocity of after the lane change, and L and W are the longitudinal displacement and lateral displacement of the vehicle at the starting and ending of the lane change, respectively.

When $v_1 = v_2 = V$, that is, when the vehicle speed at the starting and ending of the lane change remains constant, the vehicle trajectory by a 5th-degree polynomial can be obtained as follows:

$$\begin{cases} x(t) = VT + (L - VT)\left(10\left(\frac{t}{T}\right)^3 - 15\left(\frac{t}{T}\right)^4 + 6\left(\frac{t}{T}\right)^5\right) \\ y(t) = W\left(10\left(\frac{t}{T}\right)^3 - 15\left(\frac{t}{T}\right)^4 + 6\left(\frac{t}{T}\right)^5\right) \end{cases} \tag{4}$$

where T indicates the length of time for the lane change, i.e., $T = t_f - t_s$. The corresponding boundary conditions that must be satisfied for vehicle lane changing are as (3), without considering jerk constraints, which can be referred to [1,50]. The boundary conditions for 7th-degree polynomial that must be satisfied for vehicle lane changing are as follows:

$$\begin{cases} x(t_s) = 0, \dot{x}(t_s) = v_1, \ddot{x}(t_s) = 0, \dddot{x}(t_s) = 0, x\left(t_f\right) = L, \dot{x}\left(t_f\right) = v_2, \ddot{x}\left(t_f\right) = 0, \dddot{x}\left(t_f\right) = 0 \\ y(t_s) = 0, \dot{y}(t_s) = 0, \ddot{y}(t_s) = 0, \dddot{y}(t_s) = 0, y\left(t_f\right) = W, \dot{y}\left(t_f\right) = 0, \ddot{y}\left(t_f\right) = 0, \dddot{y}\left(t_f\right) = 0 \end{cases} \tag{5}$$

$$\begin{cases} m_0 = 0 \\ m_1T + m_2T^2 + m_3T^3 + m_4T^4 + m_5T^5 + m_6T^6 + m_7T^7 = L \\ m_1 = V \\ m_1 + 2m_2T + 3m_3T^2 + 4m_4T^3 + 5m_5T^4 + 6m_6T^5 + 7m_7T^6 = V \\ m_2 = 0 \\ 6m_3T + 12m_4T^2 + 20m_5T^3 + 30m_6T^4 + 42m_7T^5 = 0 \\ m_3 = 0 \\ 24m_4T + 60m_5T^2 + 120m_6T^3 + 210m_7T^4 = 0 \end{cases} \tag{6}$$

$$\begin{cases} n_0 = 0 \\ n_1T + n_2T^2 + n_3T^3 + n_4T^4 + n_5T^5 + n_6T^6 + n_7T^7 = W \\ n_1 = 0 \\ n_1 + 2n_2T + 3n_3T^2 + 4n_4T^3 + 5n_5T^4 + 6n_6T^5 + 7n_7T^6 = 0 \\ n_2 = 0 \\ 6n_3T + 12n_4T^2 + 20n_5T^3 + 30n_6T^4 + 42n_7T^5 = 0 \\ n_3 = 0 \\ 24n_4T + 60n_5T^2 + 120n_6T^3 + 210n_7T^4 = 0 \end{cases} \tag{7}$$

Let $t_s = 0$ and $t_f = T$, with $v_1 = v_2 = V$. Expanding the longitudinal displacement equation in (5) leads to (6). Similarly, expanding the lateral displacement equation in (5) results in (7). Finally, the vehicle trajectory by a 7th-degree polynomial can be acquired as follows:

$$\begin{cases} x(t) = VT + (L - VT)\left(35\left(\frac{t}{T}\right)^4 - 84\left(\frac{t}{T}\right)^5 + 70\left(\frac{t}{T}\right)^6 - 20\left(\frac{t}{T}\right)^7\right) \\ y(t) = W\left(35\left(\frac{t}{T}\right)^4 - 84\left(\frac{t}{T}\right)^5 + 70\left(\frac{t}{T}\right)^6 - 20\left(\frac{t}{T}\right)^7\right) \end{cases} \tag{8}$$

3.2. Comparison Between Quintic Polynomials and 7th-Degree Polynomials

The vehicle peak lateral acceleration and lateral jerk are closely related to the lane change trajectory, specifically determined by Equation (5). By solving for the lane change duration, the peak lateral acceleration and lateral jerk corresponding to that duration can be derived. The comparison between the 5th polynomial planning trajectories and the 7th polynomial planning trajectories with different constraints are shown in Table 1. It can be concluded that in scenario ①, the shortest longitudinal distance of the single lane-changing trajectory planned by the 5th-polynomial is 35.79 m and the maneuvering time is 2.42 s, which is basically consistent with [1]. For both 5th polynomial and 7th polynomial lane-changing trajectories, the shortest longitudinal distances increase with the increase of lane width and speed, while they decrease with the lateral acceleration. It is also found that the shortest longitudinal distance is larger for the 7th polynomial than for the 5th polynomial under the same constraints and the maneuvering time is correspondingly longer. For example, under scenario ③, when the vehicle longitudinal velocity is 20 m/s, the lane width is 3.5 m, and the maximum lateral acceleration does not increase beyond 3 m/s^2, the shortest longitudinal distance of the 5th polynomial planning trajectory is 51.67 m, and the maneuvering time is 2.61 s, while the shortest longitudinal distance of the 7thpolynomial planning trajectory is 59.0 m, and the maneuvering time is 2.97 s. It is worth noting that, by solving constrained optimization problems, the maneuvering time T can be determined. For more details, please refer to reference [1].

Table 1. Longitudinal displacement and maneuvering duration for lane changes under the constraints of different speeds, lane widths, and maximum lateral accelerations.

Scenarios	V (m/s)	W (m)	A (m/s^2)	L (m)		T (s)	
				Quintic	Seventh	Quintic	Seventh
①	15	3	3	35.79	40.89	2.42	2.76
②	15	3.5	3	38.61	44.13	2.62	2.98
③	20	3.5	3	51.67	59.0	2.61	2.97
④	20	3.5	5	39.90	45.6	2.03	2.31

The results of the 5th and 7th polynomial trajectory planning under the four different scenarios are depicted in Figures 3 and 4, respectively. It can be derived that the jerk value of the 7th polynomial trajectory is significantly lower than that of the 5th polynomial trajectory under the same constraints, so the comfort of the vehicle is significantly improved by using the 7th polynomial under sufficient longitudinal distance. Under scenario ④, the maximum jerk value of the 5th polynomial trajectory is 25 m/s^3, which occurs at the starting and ending moments of the lane change, while the maximum jerk value of the 7th polynomial trajectory is 15 m/s^3, which occurs during the intermediate phase of the lane change. Taking Scene ③ in Table 1 as an example, the comparison results of the 5th-order and 7th-order polynomial trajectory planning are shown in Figure 5. It can be seen that the lateral jerk response is significantly improved with the 7th-order polynomial.

A comparison between the 5th polynomial and the 7th polynomial planning trajectories with different jerk constraints is shown in Table 2. The results under four different scenarios with 5th polynomial and 7th polynomial trajectories are demonstrated in Figures 6 and 7, respectively. It can be noticed that, under the condition of the same lateral jerk constraint, the shortest longitudinal distance required for lane changing is more frequent at higher speeds and wider lanes. Provided that vehicle speed and lane width are the same, there is a corresponding decrease in the shortest longitudinal distance required for lane changing as the maximum lateral jerk value increases. Under the same constraints, the longitudinal distance of the 7th polynomial planning trajectory is slightly smaller than that of the 5th polynomial, and there is a corresponding reduction in the maneuver time. Taking Scene ③ in Table 2 as an example, the comparison results of the 5th-order and

7th-order polynomial trajectory planning are shown in Figure 8. Under these constraint conditions, the lateral velocity and lateral acceleration are slightly higher with the 7th-order polynomial compared to the 5th-order polynomial.

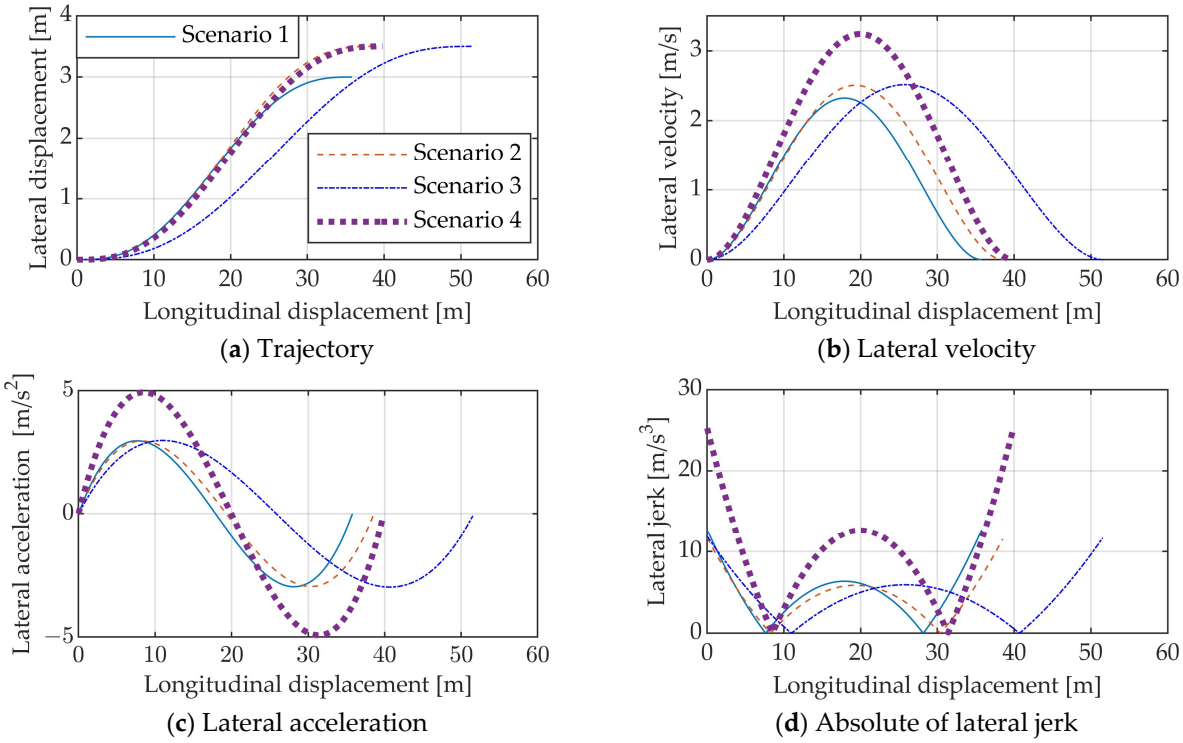

(**a**) Trajectory (**b**) Lateral velocity

(**c**) Lateral acceleration (**d**) Absolute of lateral jerk

Figure 3. Trajectory planned by 5th polynomial (under the constraints of speed, lane width, and lateral acceleration).

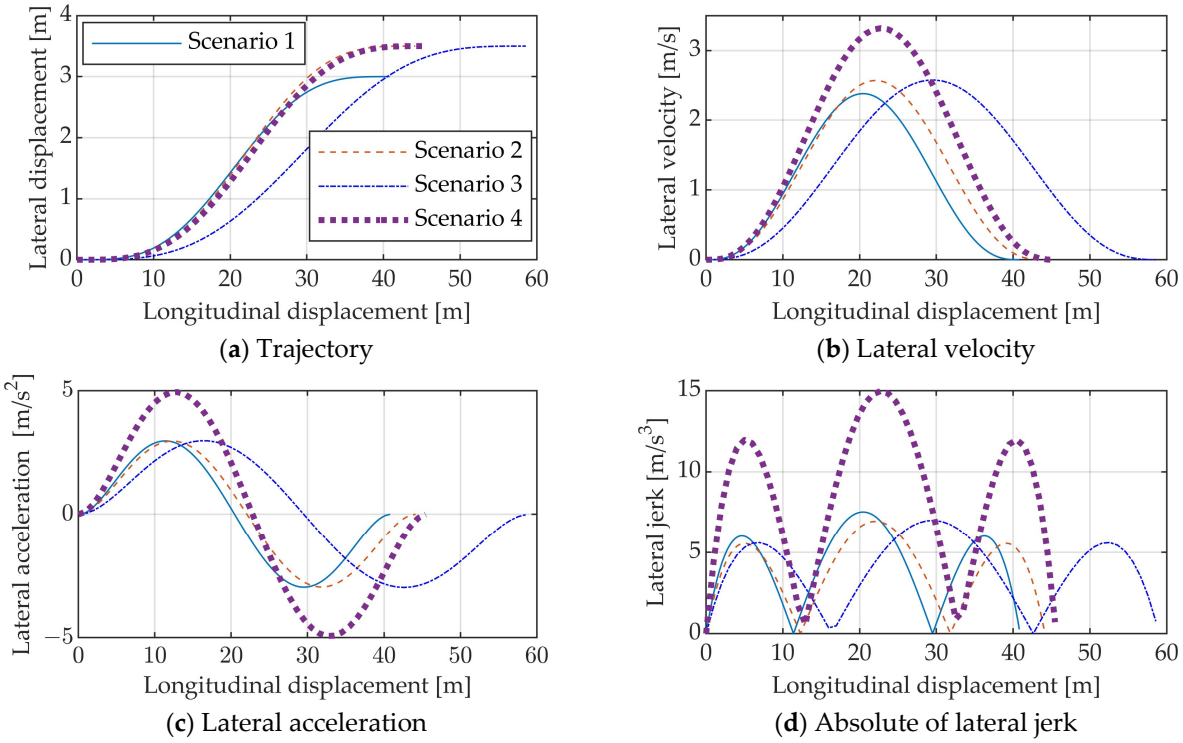

(**a**) Trajectory (**b**) Lateral velocity

(**c**) Lateral acceleration (**d**) Absolute of lateral jerk

Figure 4. Trajectory planned by 7th polynomial (under the constraints of speed, lane width, and lateral acceleration).

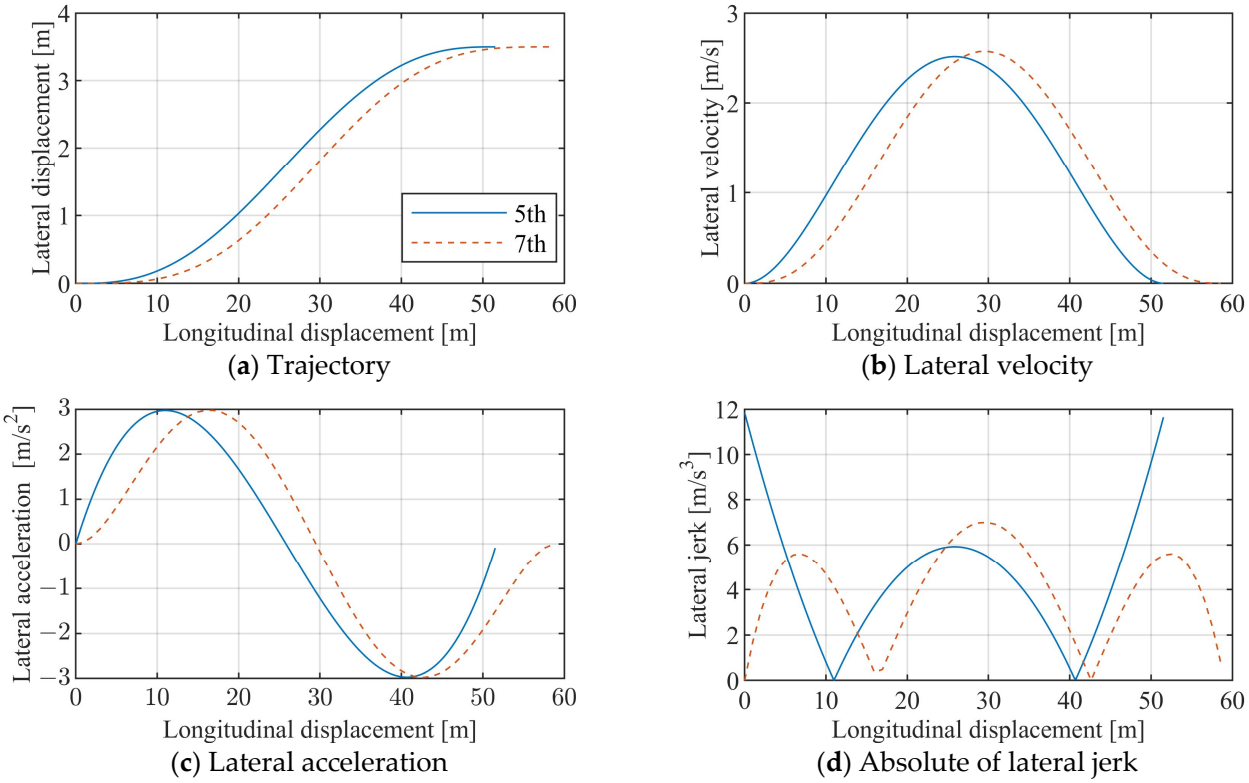

Figure 5. Results of 5th polynomial and 7th polynomial (V = 20 m/s, W = 3.5 m, A = 3 m/s^2).

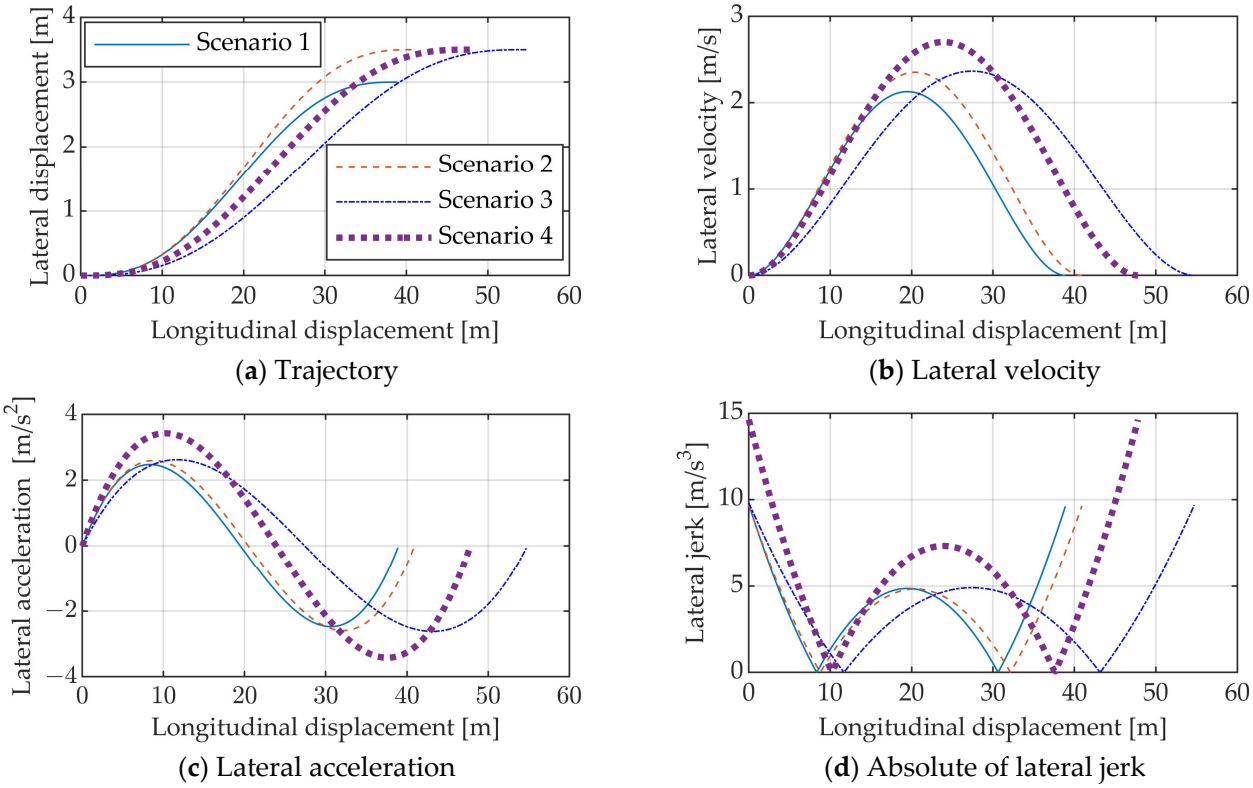

Figure 6. Trajectory planned by 5th polynomial (under the constraints of speed, lane width and lateral jerk).

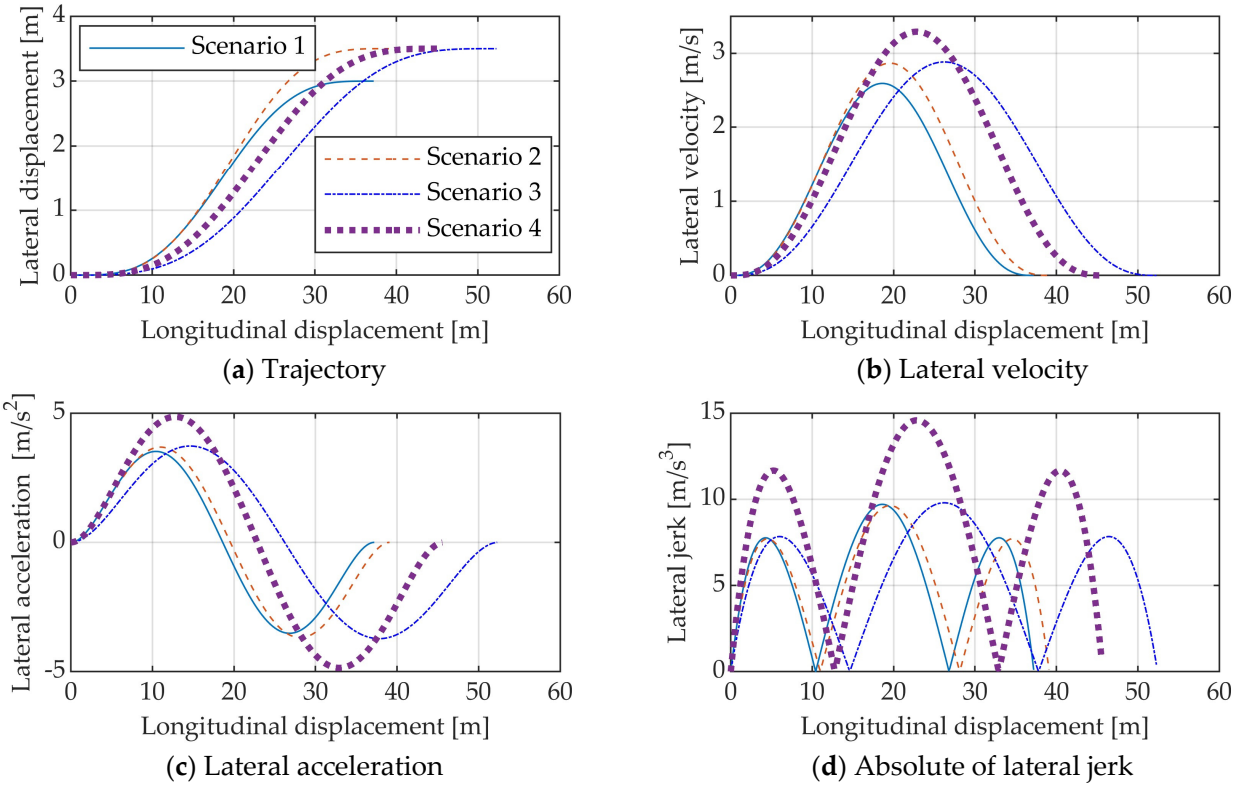

Figure 7. Trajectory planned by 7th polynomial (under the constraints of speed, lane width and lateral jerk).

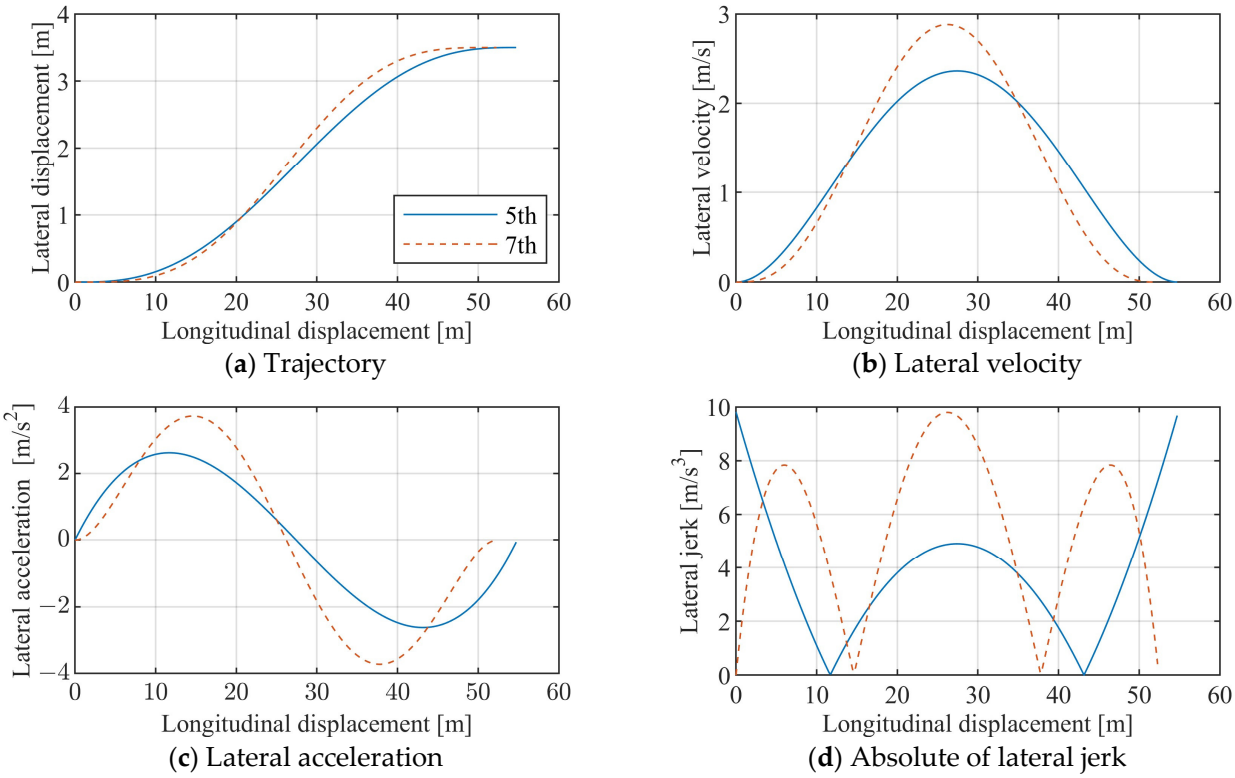

Figure 8. Results of 5th polynomial and 7th polynomial (V = 20 m/s, W = 3.5 m, $Jerk\_y$ = 10 m/s^3).

Table 2. Longitudinal displacement and maneuvering duration for lane changes under the constraints of different speeds, lane widths, and maximum lateral jerks.

Scenarios	*V* (m/s)	*W* (m)	*Jerk_y* (m/s^3)	*L* (m)		*T* (s)	
				Quintic	Seventh	Quintic	Seventh
①	15	3	10	38.96	37.23	2.65	2.53
②	15	3.5	10	40.93	39.10	2.79	2.67
③	20	3.5	10	54.84	52.42	2.78	2.66
④	20	3.5	15	47.81	45.69	2.43	2.33

3.3. MPTC by Four-Wheel Steering

3.3.1. Vehicle Dynamics Model

A simplified 2 DOF vehicle dynamics model, depicted in Figure 9, is employed in this study. The model assumes a ground-level center of gravity and small-angle approximations for the wheel steering angles. The governing equations for lateral and yaw motion are presented below [28,51].

$$mV(\dot{\beta} + r) = 2C_f(\delta_f - \frac{l_f r}{V} - \beta) + 2C_r(\delta_r - \frac{l_f r}{V} - \beta) \tag{9}$$

$$I_z\dot{r} = 2C_f l_f(\delta_f - \frac{l_f r}{V} - \beta) - 2C_r l_r(\delta_r - \frac{l_f r}{V} - \beta) \tag{10}$$

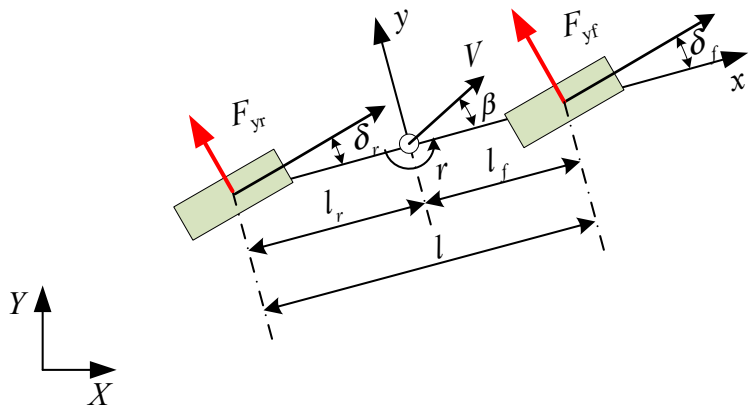

Figure 9. Vehicle 2 DOF model.

The following notation is used throughout this study: V represents the vehicle velocity; δ_f, δ_r are the front and rear wheel steering angles; β is vehicle sideslip angle; r is the yaw rate; F_{yf} and F_{yr} are the front and rear tire lateral forces; l_f and l_r are the distances from the center of gravity to the front and rear axles; m is vehicle mass; and I_z is yaw moment of inertia. C_f, C_r denote the front and rear tire cornering stiffnesses.

3.3.2. Controller Design

A model predictive control method is chosen for designing the 4WS controller. The MPC controller design of front-wheel steering is similar to the four-wheel steering, but without rear-wheel steering. It will not be introduced here, and the details can be referred to [31]. MPC's ability to handle constraints and predict future behavior makes it well-suited for accurate lateral tracking control. The state equation for the 2-DOF vehicle model is expressed as follows:

$$\begin{aligned} \dot{x} &= Ax + Bu \\ y &= Cx + Du \end{aligned} \tag{11}$$

where the system state variable vector $x = [Y, \psi, v_y, r]^T$, the feedback controller input $u = [\delta_f, \delta_r]^T$ is given to the vehicle modeling module, the system output $y = [\psi, Y]^T$. ψ is the course angle of the vehicle, and Y is the lateral displacement in the absolute coordinate system.

$$A = \begin{bmatrix} 0 & V & 1 & 0 \\ 0 & 0 & 0 & 1 \\ 0 & 0 & -\frac{C_f+C_r}{mV} & \frac{l_rC_r-l_fC_f}{mV} - V \\ 0 & 0 & \frac{l_rC_r-l_fC_f}{I_zV} & -\frac{l_f^2C_f+l_r^2C_r}{I_zV} \end{bmatrix}, B = \begin{bmatrix} 0 & 0 \\ 0 & 0 \\ -\frac{C_f}{m} & -\frac{C_r}{m} \\ -\frac{l_fC_f}{I_z} & \frac{l_rC_r}{I_z} \end{bmatrix}, C = \begin{bmatrix} 0 & 1 & 0 & 0 \\ 1 & 0 & 0 & 0 \end{bmatrix}, D = \begin{bmatrix} 0 & 0 \\ 0 & 0 \end{bmatrix}.$$

The vehicle dynamics model in Equation (11) is linearly discretized by performing a first-order Taylor expansion around an arbitrary operating point (x_r, u_r) and subtracting it from the original state, yielding the following state error equation:

$$\dot{e} = \begin{bmatrix} \dot{Y} - \dot{Y}_r \\ \dot{\psi} - \dot{\psi}_r \\ \dot{v}_y - \dot{v}_{yr} \\ \dot{r} - \dot{r}_r \end{bmatrix} = A(t) \begin{bmatrix} Y - Y_r \\ \psi - \psi_r \\ v_y - v_{yr} \\ r - r_r \end{bmatrix} + B(t) \begin{bmatrix} \delta_f - \delta_{fr} \\ \delta_r - \delta_{rr} \end{bmatrix} \tag{12}$$

where $A(t) = A$, $B(t) = B$. By applying the first-order finite difference method to discretize the above equation, we obtain:

$$\begin{cases} e(k+1) = A(k)e(k) + B(k)\Delta u(k) \\ \Delta y(k) = C(k)e(k) + D(k)\Delta u(k) \end{cases} \tag{13}$$

where $A(k) = I + \tau A(t)$, $B(k) = \tau B(t)$, $C(k) = C$, $D(k) = D$. τ is the sampling time. By combining the discrete state variable and control variable into a new state variable, we obtain:

$$\xi(k) = \begin{bmatrix} e(k) \\ u(k-1) \end{bmatrix} \tag{14}$$

We further obtain the new discrete state–space representation as follows:

$$\begin{cases} \xi(k+1) = \widetilde{A}(k)\xi(k) + \widetilde{B}(k)\Delta u(k) \\ y(k) = \widetilde{C}(k)\xi(k) + \widetilde{D}(k)\Delta u(k) \end{cases} \tag{15}$$

where $\widetilde{A}(k) = \begin{bmatrix} A(k) & B(k) \\ O_{2\times4} & I_2 \end{bmatrix}$, $\widetilde{B}(k) = \begin{bmatrix} B(k) \\ I_2 \end{bmatrix}$, $\widetilde{C}(k) = \begin{bmatrix} C(k) & O_{2\times2} \end{bmatrix}$, $\widetilde{D}(k) = [D(k)]$.

By utilizing the predictive model and constraints, the system state deviations and control inputs are optimized, leading to the following objective function:

$$J(k) = \sum_{i=1}^{N_p} \| y(k+i|t) - y_r(k+i|t) \|_Q^2 + \sum_{i=0}^{N_c-1} \| \Delta u(k+i|t) \|_R^2 + \rho\varepsilon^2 \tag{16}$$

N_p, N_c denotes the time horizon for prediction and the time horizon for control, respectively; Q is the state regulation matrix; R is the control input regulation matrix; ε is the relaxation factor; and ρ denotes the relaxation factor regulation coefficient. For the four-wheel steering system, the weighting matrices are denoted as $Q_{4\mathrm{ws}}$ and $R_{4\mathrm{ws}}$.

By solving the objective function, the control increment sequence at time step k can be obtained as follows:

$$\Delta U(k) = [\Delta u(k), \Delta u(k+1), \cdots, \Delta u(k+N_c-1)]^T \tag{17}$$

The control variable at time step k can be expressed as the control variable at time step $k-1$ plus the control increment at time step k, as follows:

$$u(k) = u(k-1) + \Delta u(k) \tag{18}$$

The expression above represents the feedback correction part of the model predictive control. By performing rolling optimization using the objective function and constraints, the control input sequence is obtained. The first value of the output sequence is then used as the input for the system at the next time step, and the process repeats for the subsequent sampling period. In each control step of the MPC, constraints can be added for the system control variables and control increments. In path tracking control, the MPC can handle the vehicle system physical constraints and provide future references from the predefined path. Constraint conditions must be satisfied as follows:

$$\begin{cases} \min\limits_{\Delta U(k)} [J(k), \Delta u(k)] \\ u_{min} \le u(k+i|k) \le u_{\max} \\ \Delta u_{min} \le \Delta u(k+i|k) \le \Delta u_{\max} \\ \varepsilon > 0 \end{cases} \tag{19}$$

where $u_{\max}$ and $u_{\min}$ are the maximum and minimum allowable values for the control inputs, respectively, corresponding to the boundary values of the front-wheel steering angle. $\Delta u_{\max}$ and $\Delta u_{\min}$ are the maximum and minimum values of the control increment, respectively. The constraints are as follows: the maximum steering angles for both the front and rear wheels are set to 0.78 radians, with a maximum rate of 0.19 radians per second.

4. Simulation and Analysis

To verify the proposed control algorithm, we simulate and analyze tracking control results in four scenarios using Matlab/Simulink R2022a. The equations are integrated and solved using the Runge–Kutta method with a 0.001s time step. The four scenarios are shown in Table 3. The lane width for all three scenarios is 3.5 m. In scenario I, it is assumed that the vehicle is operating on a low-friction surface, characterized by friction of μ = 0.3. The vehicle's initial velocity is 15 m/s, and the lateral acceleration that the ground can provide is limited to 3 m/s^2. In scenario II, given that the vehicle runs on a moderate adhesion surface (μ = 0.5), the vehicle lateral acceleration that the ground can provide is limited to 5 m/s^2, and the initial velocity is 17 m/s. In the third scenario, assuming that the vehicle is traveling on a high adhesion surface (μ = 1.0) at the speed of 20 m/s, the maximum lateral jerk does not exceed 10 m/s^3, in order to ensure that the passengers have better comfort during the lane change maneuver. In the scenario IV, it is assumed that the vehicle is traveling on a high adhesion surface (μ = 1.0) at the speed of 30 m/s, and the maximum lateral jerk does not exceed 15 m/s^3. Table 4 presents a comprehensive list of the vehicle model and controller parameters.

Table 3. Scenarios for simulation.

Scenarios	*V* (m/s)	*W* (m)	Constraint Conditions	
			A (m/s^2)	*Jerk_y* (m/s^3)
I	15	3.5	3	—
II	17	3.5	5	—
III	20	3.5	—	10
IV	30	3.5	—	15

Table 4. Main parameters of vehicle model and controller.

Symbol	Parameter Specification	Value/Unit
m	Vehicle mass	1500/kg
l_f	Distance between the center of gravity and the front axle	1.2/m
l_r	Distance between the center of gravity and the rear axle	1.3/m
I_z	Yaw inertia moment	3000/(kg·m^2)
C_f	Front axle cornering stiffness	50,000/(N·m^{-1})
C_r	Rear axle cornering stiffness	70,000/(N·m^{-1})
N_p	Time domain for prediction	12
N_c	Time domain for control	3
τ	Sampling time	0.02/s
Q_{2ws}	State weighting matrix for 2WS	diag ([100,10,10,1])
R_{2ws}	Control weighting matrix for 2WS	diag ([1])
Q_{4ws}	State weighting matrix for 4WS	diag ([100,10,10,1])
R_{4ws}	Control weighting matrix for 4WS	diag ([1,1])
ρ	Relaxation scaling factor	1000

4.1. Scenario I

The results of the vehicle's response under Scenario I are illustrated in Figure 10. Figure 10a–g show the responses of vehicle lateral displacement, lateral displacement tracking error, sideslip angle, yaw rate, lateral acceleration, lateral jerk, and steering angles of both front and rear wheels, respectively. It can be observed that both the 4WS and 2WS systems demonstrate effective tracking of the pre-planned trajectories. However, the 2WS system exhibits marginally superior lateral displacement tracking performance. The sideslip angle response of 4WS is significantly better than that of 2WS, with a maximum value of about 0.012 rad for 4WS and 0.018 rad for 2WS. The yaw rate for 4WS is closer to the reference than that for 2WS. Although the peak value of vehicle lateral acceleration is 3 m/s^2 for both control systems, which coincides with the given constraints, the 2WS system shows significant fluctuations, resulting in sharp fluctuations in its lateral jerk, while the 4WS has a maximum lateral jerk of 8 m/s^3, which provides a significant improvement in comfort. The peak values of front and rear wheel steering angles for the 4WS are 0.07 rad and 0.03 rad, respectively. The 2WS system exhibits a maximum front wheel steering angle of 0.07 rad, but the fluctuations are more drastic compared to the 4WS.

Figure 11 shows a comparison of the computation times for the 2WS and 4WS systems on the specific hardware configuration as follows: Intel(R) Core (TM) i9-9900K CPU @ 3.60 GHz processor and 64 GB RAM. It can be observed that the computation time for the 4WS system is slightly longer than that for the 2WS system. Figure 12 presents the stability analysis results for the 2WS system. It can be seen that, when the initial sideslip angles are −0.1 rad, −0.05 rad, 0 rad, 0.05 rad, and 0.1 rad, the vehicle's yaw rate remains stable throughout the trajectory tracking process.

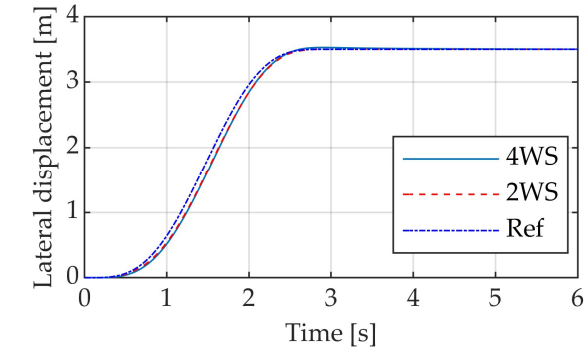

(**a**) Lateral displacement

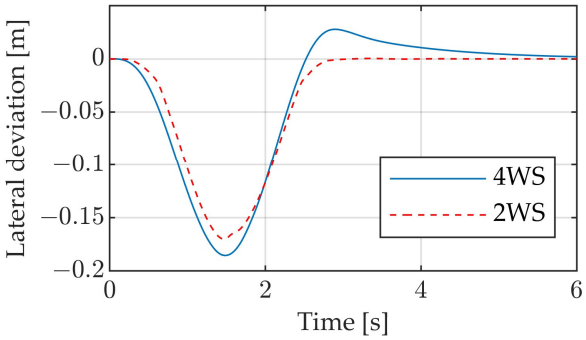

(**b**) Lateral deviation

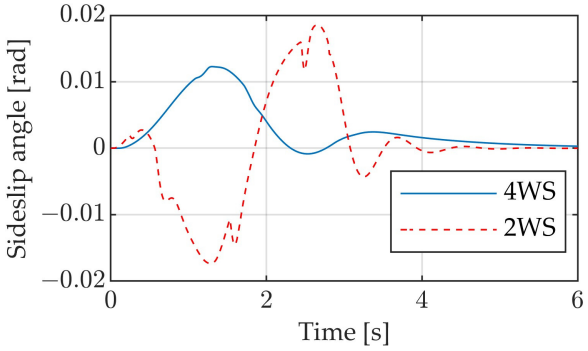

(**c**) Sideslip angle

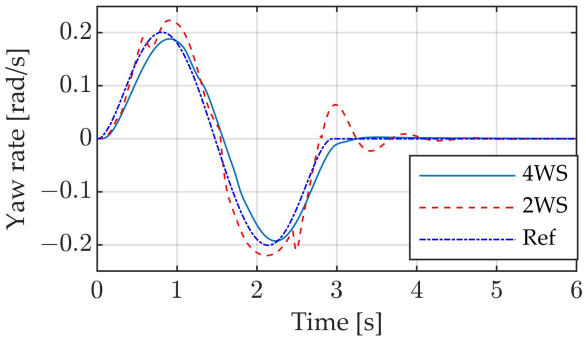

(**d**) Yaw rate

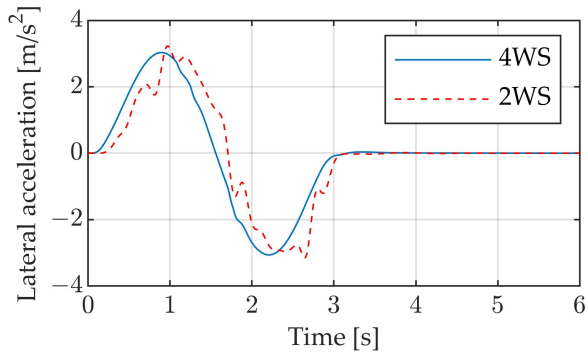

(**e**) Lateral acceleration

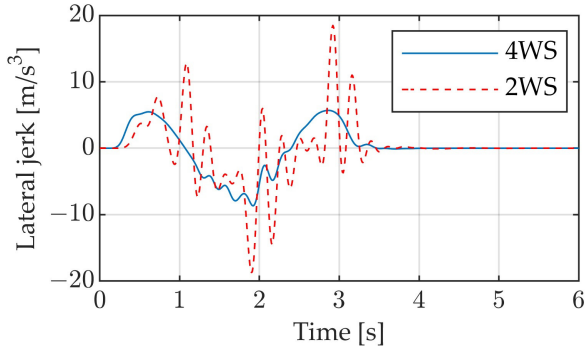

(**f**) Lateral jerk

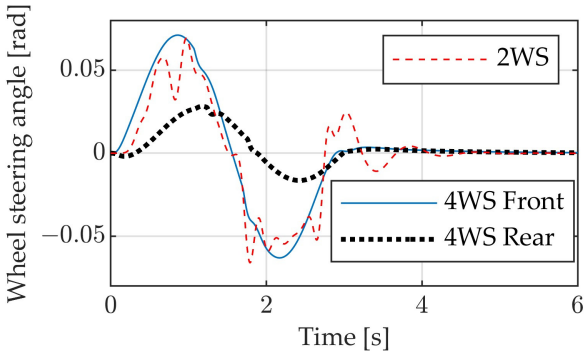

(**g**) Front and rear wheel steering angles

Figure 10. Vehicle response (v = 15 m/s, W = 3.5 m, μ = 0.3).

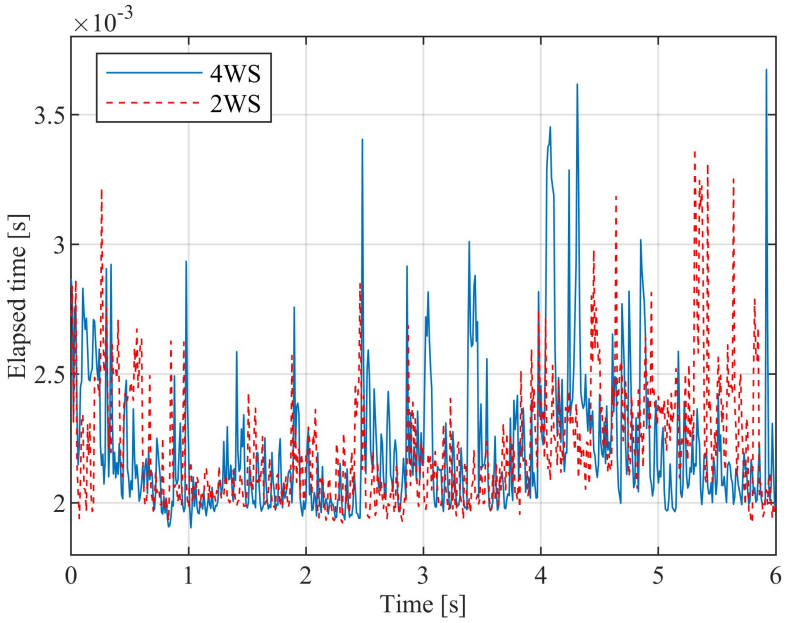

Figure 11. Comparison of calculation time between 2WS and 4WS systems.

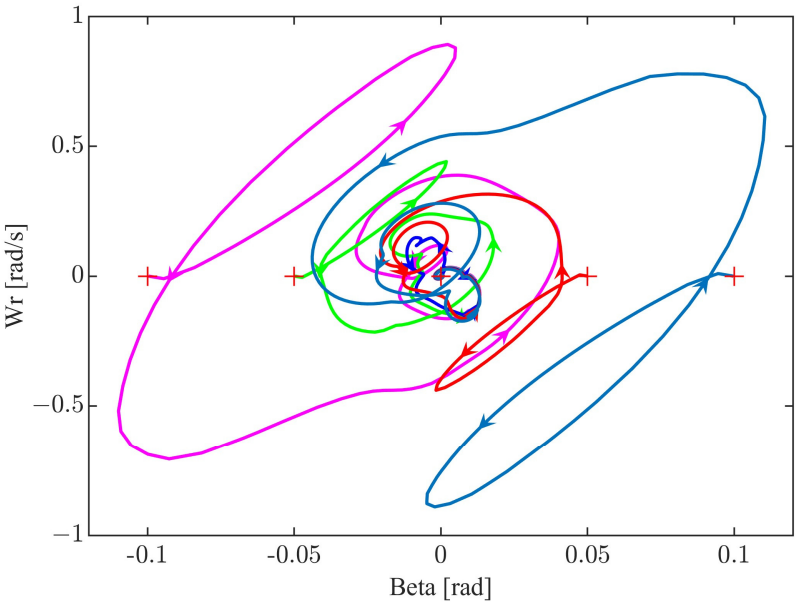

Figure 12. Stability analysis of 2WS system.

4.2. Scenario II

The results of the vehicle's response under Scenario II are presented in Figure 13. Figure 13a–g show the responses of vehicle lateral displacement, lateral displacement tracking error, sideslip angle, yaw rate, lateral acceleration, lateral jerk, and front and rear wheel steering angles, respectively. It can be noticed that the 4WS and 2WS also track the preplanned trajectory well in this scenario, with maximum lateral displacement tracking errors of 0.23 m and 0.28 m for the 4WS and 2WS, respectively. The sideslip angle of the 4WS is significantly improved compared to the 2WS, with peak values of 0.05 rad and 0.016 rad respectively. The yaw rate of the 4WS is also better than that of the 2WS, which shows a larger amount of overshoot and significant fluctuations. The lateral acceleration of the 4WS system is kept within the constraints, with a maximum value of 5 m/s^2. The 2WS lateral acceleration, on the other hand, shows significant oscillations, with a maximum value of 7.48 m/s^2, leading to sharp fluctuations in its lateral jerk as well, with a peak value

of 80 m/s^3. The maximum value of lateral jerk for 4WS is 20 m/s^3. The maximum steering angles of the front and rear wheels of the 4WS vehicle are 0.1 rad and 0.05 rad, respectively. The maximum front wheel steering angle of the 2WS vehicle is 0.25 rad and fluctuates drastically during the maneuver.

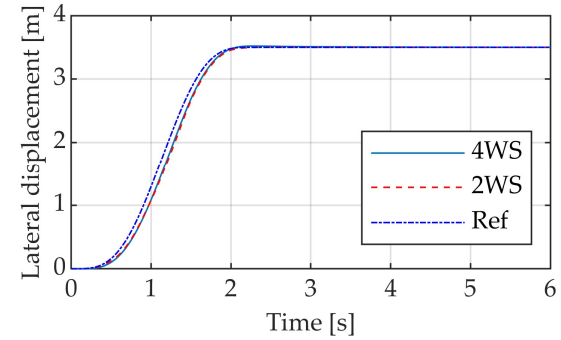

(**a**) Lateral displacement

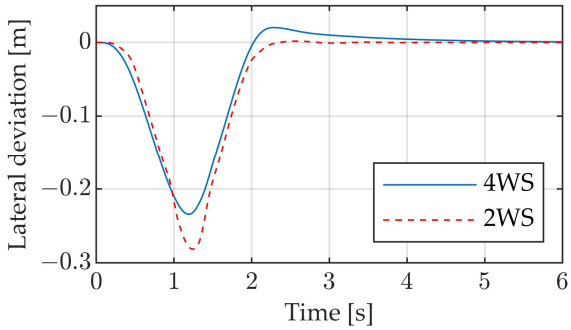

(**b**) Lateral deviation

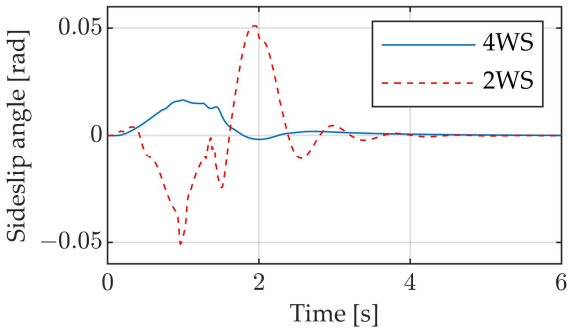

(**c**) Sideslip angle

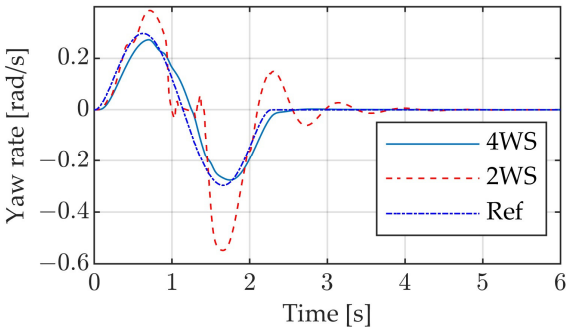

(**d**) Yaw rate

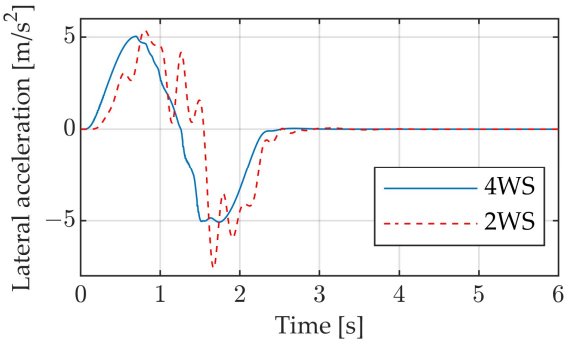

(**e**) Lateral acceleration

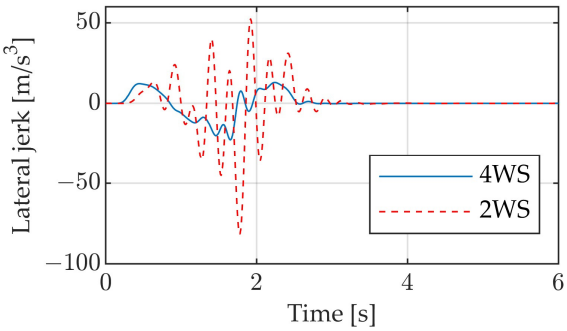

(**f**) Lateral jerk

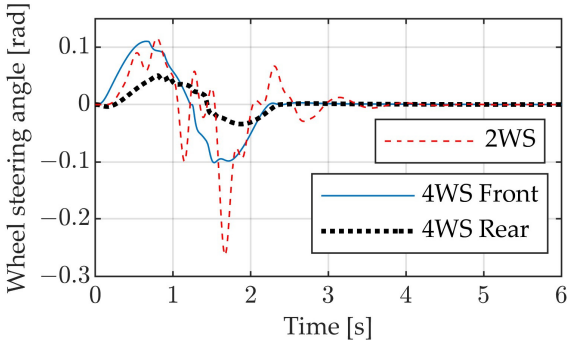

(**g**) Front and rear wheel steering angles

Figure 13. Vehicle response (v = 17 m/s, W = 3.5 m, μ = 0.5).

4.3. Scenario III

The results of the vehicle's response under Scenario III are shown in Figure 14. Figure 14a–g show the responses of vehicle lateral displacement, lateral displacement tracking error, sideslip angle, yaw rate, lateral acceleration, lateral jerk, and front and rear wheel steering angles, respectively. It can be noticed that the 4WS and 2WS can track the preplanned trajectory well in this scenario, and their maximum lateral displacement tracking errors are about 0.17 m and 0.19 m, respectively. The peak values of sideslip angle for both systems are 0.015 rad and 0.03 rad, respectively, and the latter shows sharp fluctuations. The yaw rate response is similar to the sideslip angle, with large oscillations for the 2WS system. Although both lateral acceleration peaks are around 4 m/s^2, the 2WS system shows dramatic fluctuations, resulting in a lateral jerk peak of 25 m/s^3. The lateral jerk maximum of 4WS is at 10 m/s^3, which matches the given constraints with better comfort. In addition, the maximum front and rear wheel steering angles of the 4WS system are 0.08 rad and 0.04 rad, respectively, under this working condition. Although the peak value of the front wheel steering angle of the 2WS system is slightly smaller than that of the 4WS, it shows severe fluctuations during the lane change maneuver.

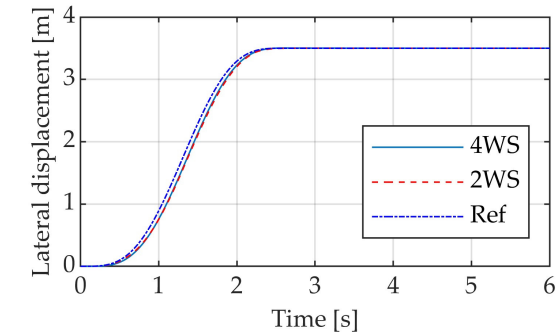

(**a**) Lateral displacement

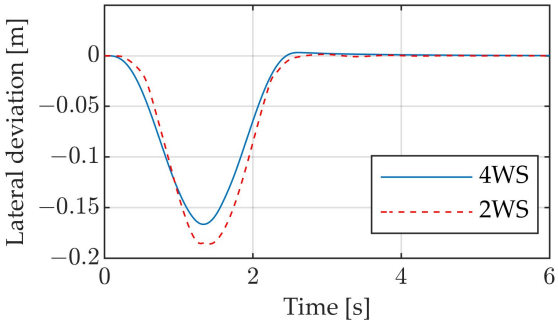

(**b**) Lateral deviation

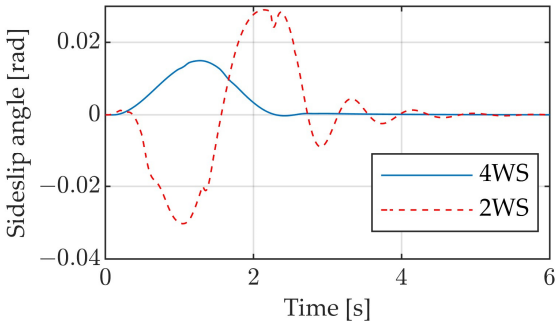

(**c**) Sideslip angle

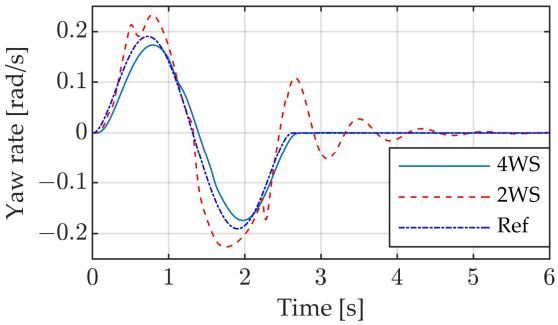

(**d**) Yaw rate

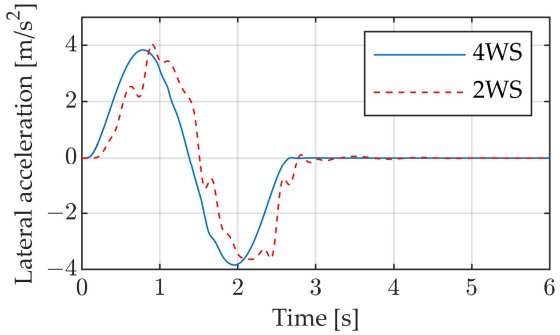

(**e**) Lateral acceleration

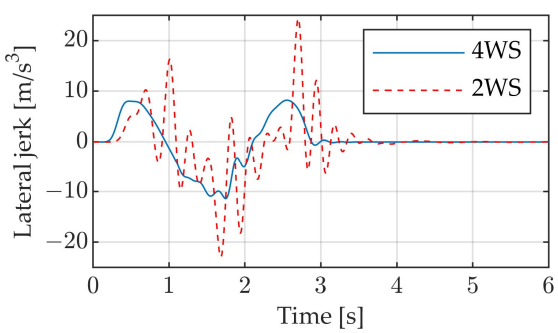

(**f**) Lateral jerk

Figure 14. *Cont.*

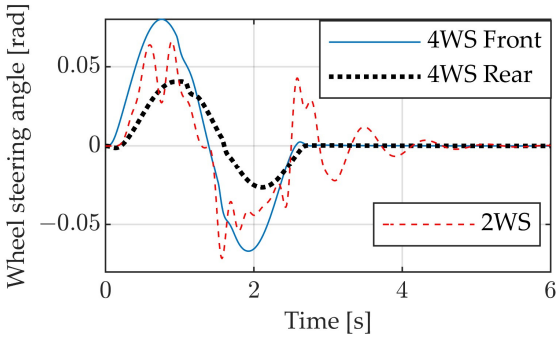

(**g**) Front and rear wheel steering angles

Figure 14. Vehicle response (v = 20 m/s, W = 3.5 m, μ = 1.0).

The simulation comparison of the above three scenarios indicates that, for the same preplanned trajectory, the 4WS has better overall performance than the 2WS. Although the 2WS can also track the planned trajectory, due to the impact of vehicle dynamics, the yaw rate and lateral acceleration will fluctuate during the maneuver, resulting in a larger lateral jerk and less comfort than the 4WS.

Figure 15 compares the responses of the nominal 4WS system and the 4WS system, of which both the vehicle mass and yaw moment of inertia are increased by 20%. Here, "4WS" refers to the nominal system response, while "4WS2" represents the system response after the change in vehicle mass and yaw moment of inertia. It can be observed that, even with an increase in vehicle mass and yaw moment of inertia, the 4WS system is still able to effectively track the desired trajectory. Compared to the nominal system, after the vehicle mass increases, the magnitude of the sideslip angle shows a slight increase, and the wheel steering angles also increase accordingly. The responses of other indicators remain consistent.

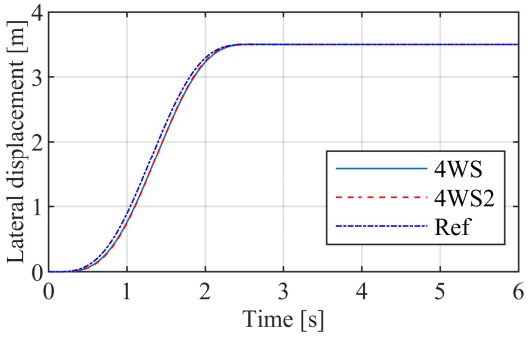

(**a**) Lateral displacement

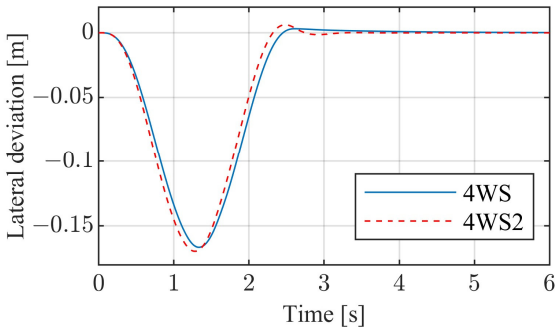

(**b**) Lateral deviation

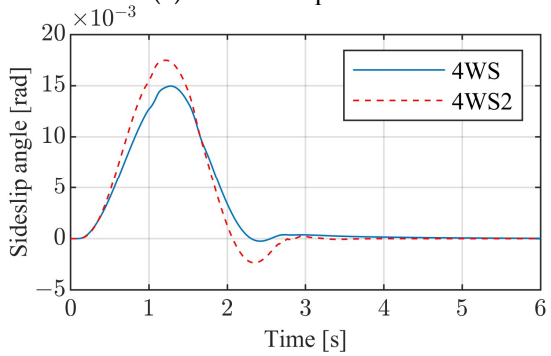

(**c**) Sideslip angle

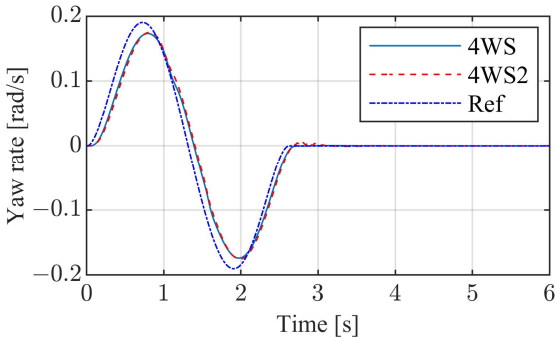

(**d**) Yaw rate

Figure 15. *Cont.*

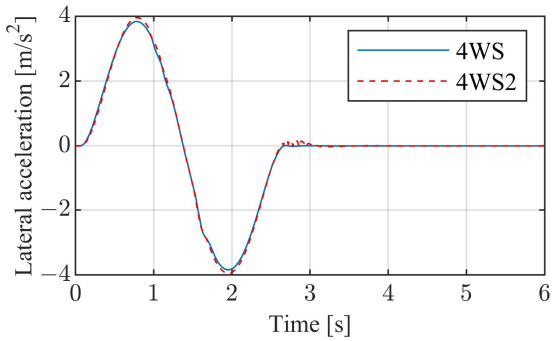

(**e**) Lateral acceleration

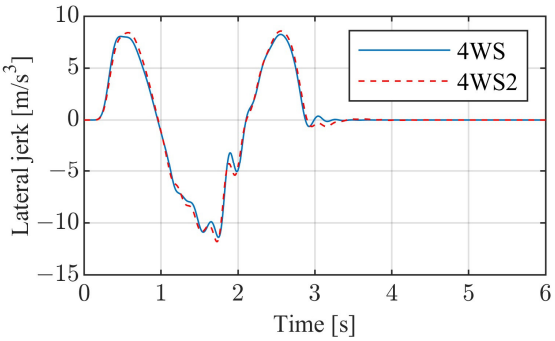

(**f**) Lateral jerk

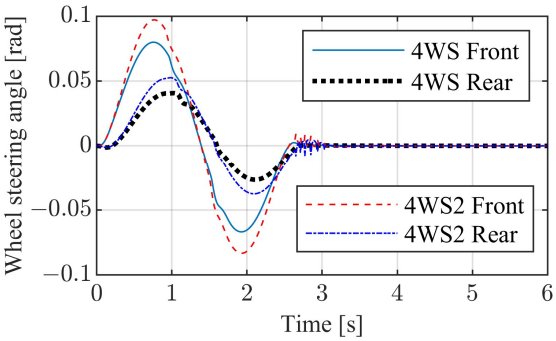

(**g**) Front and rear wheel steering angles

Figure 15. Vehicle response (v = 20 m/s, W = 3.5 m, μ = 1.0).

4.4. Scenario IV

The results of the vehicle's response under Scenario IV are shown in Figure 16. Figure 16a–g show the responses of vehicle lateral displacement, lateral displacement tracking error, sideslip angle, yaw rate, lateral acceleration, lateral jerk, and front and rear wheel steering angles, respectively. It can be noticed that the 4WS system can track the preplanned trajectory well in this scenario, and its maximum lateral displacement tracking error is about 0.15 m. The peak value of sideslip angle is about 0.025 rad. The lateral jerk maximum is at 15 m/s^3, which matches the given constraints with better comfort. In addition, the maximum front and rear wheel steering angles of the 4WS system are 0.1 rad and 0.06 rad, respectively.

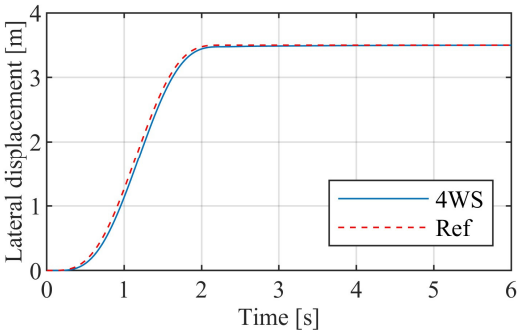

(**a**) Lateral displacement

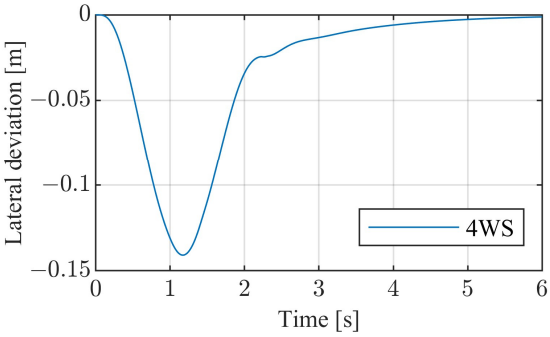

(**b**) Lateral deviation

Figure 16. *Cont.*

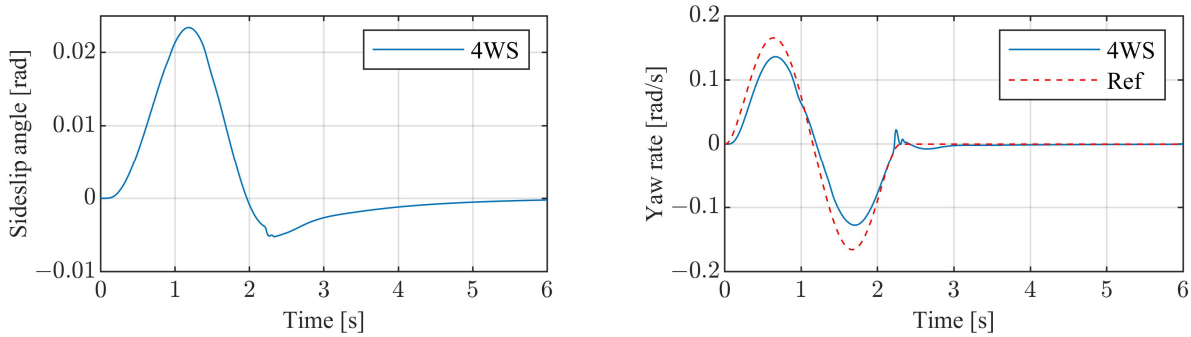

(**c**) Sideslip angle

(**d**) Yaw rate

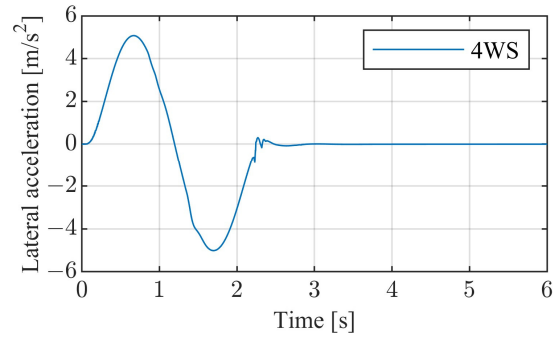

(**e**) Lateral acceleration

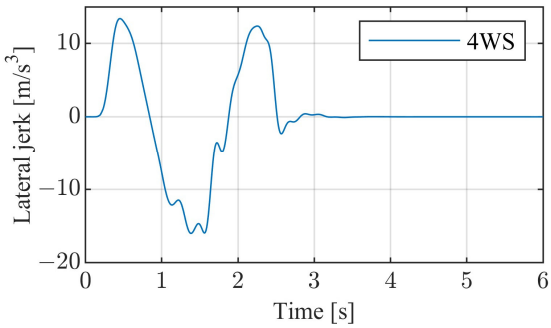

(**f**) Lateral jerk

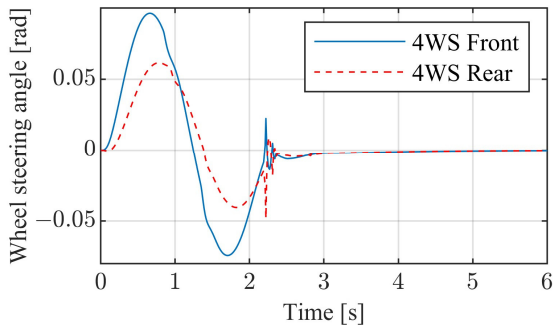

(**g**) Front and rear wheel steering angles

Figure 16. Vehicle response (v = 30 m/s, W = 3.5 m, μ = 1.0).

5. Conclusions

In this study, planning and tracking control of single lane change trajectories are carried out, with trajectory planning using 5th-order polynomial and 7th-order polynomials, and tracking control using four-wheel steering MPC and front-wheel steering MPC. The following conclusions are drawn:

(1) With sufficient longitudinal distance for lane changing, the 7th polynomial trajectory provides better comfort compared to the 5th polynomial trajectory.

(2) For the same planned trajectory, there is a substantial difference in the vehicle response when different control methods are used for tracking. In comparison with the front-wheel steering MPC system, the overall performance of the four-wheel steering MPC system is greatly improved, with significant improvements in the sideslip angle and lateral jerk under different constraints.

It is worth noting that the algorithm presented in this study has only been validated through simulations under ideal constraint conditions and it purely explores, from a theoretical perspective, the control method that combines 7th-order polynomials with MPC for four-wheel steering. The proposed control algorithm will be further validated by field test in the future. For static and dynamic obstacles, information about the obstacles (such as displacement, velocity, and acceleration) needs to be determined based on sensor data.

This information can then be translated into constraint conditions, which are subsequently used for trajectory planning. Other factors, such as the impact of nominal parameters, the real-time system performance, and the design of fail-safe mechanisms, will be taken into account during the real-world validation process.

Author Contributions: Conceptualization, F.L.; methodology, formal analysis, F.L. and C.H.; software, validation, F.L.; writing, F.L. and C.H.; supervision, project administration, F.L. All authors have read and agreed to the published version of the manuscript.

Funding: This work was supported by National Natural Science Foundation of China (NSFC) Project (52472400), Chongqing Natural Science Foundation Project (CSTB2024NSCQ-MSX0493), Science and Technology Research Program of Chongqing Education Commission of China (KJZD-K202404001), and Chongqing University of Technology Undergraduate Education and Teaching Reform Research Project (2024YB09).

Data Availability Statement: Data are contained within the article.

Conflicts of Interest: The authors declare no conflicts of interest.

References

1. Shamir, T. How should an Autonomous Vehicle Overtake a Slower Moving Vehicle: Design and Analysis of an Optimal Trajectory. *IEEE Trans. Autom. Control* **2004**, *49*, 607–610. [CrossRef]
2. Shiller, Z.; Sundar, S. Emergency Lane-Change Maneuvers of Autonomous Vehicles. *J. Dyn. Syst. Meas. Control* **1998**, *120*, 37–44. [CrossRef]
3. Anisi, D.; Hamberg, J.; Hu, X. Nearly Time-Optimal Paths for a Ground Vehicle. *J. Control Theory Appl.* **2003**, *1*, 2–8. [CrossRef]
4. Singh, A.; Putra, A.; Kassim, K. Time to Collision for Emergency Obstacle Avoidance. *J. Soc. Automot. Eng. Malays.* **2021**, *5*, 223–234. [CrossRef]
5. Tomar, R.; Verma, S. Safety of Lane Change Maneuver Through a Priori Prediction of Trajectory Using Neural Networks. *Netw. Protoc. Algorithms* **2012**, *4*, 4–21. [CrossRef]
6. Analooee, A.; Kazemi, R.; Azadi, S. SCR-Normalize: A Novel Trajectory Planning Method based on Explicit Quintic Polynomial Curves. *Proc. Inst. Mech. Eng. Part K J. Multi-Body Dyn.* **2020**, *234*, 650–674. [CrossRef]
7. Yamada, Y.; Bakibillah, A.S.M.; Hashikura, K. Autonomous Vehicle Overtaking Modeling and an Optimal Trajectory Generation Scheme. *Sustainability* **2022**, *14*, 1807. [CrossRef]
8. Nemeth, B.; Gáspár, P.; Hegedűs, T. Optimal Control of Overtaking Maneuver for Intelligent Vehicles. *J. Adv. Transp.* **2018**, *1*, 2195760. [CrossRef]
9. Garrido, F.; González, L.; Milanés, V. A Two-Stage Real-Time Path Planning: Application to the Overtaking Manuever. *IEEE Access* **2020**, *8*, 128730–128740. [CrossRef]
10. Lattarulo, R.; Rastelli, J. A Hybrid Planning Approach based on MPC and Parametric Curves for Overtaking Maneuvers. *Sensors* **2021**, *21*, 595. [CrossRef] [PubMed]
11. Karimshoushtari, M.; Novara, C.; Tango, F. How Imitation Learning and Human Factors Can Be Combined in a Model Predictive Control Algorithm for Adaptive Motion Planning and Control. *Sensors* **2021**, *21*, 4012. [CrossRef] [PubMed]
12. Kim, J.; Pae, D.; Lim, M. Obstacle Avoidance Path Planning based on Output Constrained Model Predictive Control. *Int. J. Control Autom. Syst.* **2019**, *17*, 2850–2861. [CrossRef]
13. Micheli, F.; Bersani, M.; Arrigoni, S. NMPC Trajectory Planner for Urban Autonomous Driving. *Veh. Syst. Dyn.* **2023**, *61*, 1387–1409. [CrossRef]
14. Li, X.; Guo, Z.; Su, D. Time-dependent Lane Change Trajectory Optimisation Considering Comfort and Efficiency for Lateral Collision Avoidance. *IET Intell. Transp. Syst.* **2021**, *15*, 595–605. [CrossRef]
15. Gabarrón, J.; Lopez, E.; Haro, J. Vehicular Trajectory Optimization for Cooperative Collision Avoidance at High Speeds. *IEEE Trans. Intell. Transp. Syst.* **2013**, *14*, 1930–1941. [CrossRef]
16. Kanchwala, H.; Viana, Í.; Aouf, N. Cooperative Path-Planning and Tracking Controller Evaluation Using Vehicle Models of Varying Complexities. *Proc. Inst. Mech. Eng. Part C J. Mech. Eng. Sci.* **2021**, *235*, 2877–2896. [CrossRef]
17. Bharilya, V.; Kumar, N. Machine Learning for Autonomous Vehicle's Trajectory Prediction: A Comprehensive Survey, Challenges, and Future Research Directions. *Veh. Commun.* **2024**, *46*, 100733. [CrossRef]
18. Karle, P.; Furtner, L.; Lienkamp, M. Self-Evaluation of Trajectory Predictors for Autonomous Driving. *Electronics* **2024**, *13*, 946. [CrossRef]
19. Raeesi, H.; Khosravi, A.; Sarhadi, P. Collision Avoidance for Autonomous Vehicles Using Reachability-based Trajectory Planning in Highway Driving. *Proc. Inst. Mech. Eng. Part D J. Automob. Eng.* **2024**. [CrossRef]
20. Piccinini, M.; Gottschalk, S.; Gerdts, M.; Biral, F. Computationally Efficient Minimum-Time Motion Primitives for Vehicle Trajectory Planning. *IEEE Open J. Intell. Transp. Syst.* **2024**, *5*, 642–655. [CrossRef]

21. Stahl, T.; Wischnewski, A.; Betz, J.; Lienkamp, M. Mutlilayer Graph-Based Trajectory Planning for Race Vehicles in Dynamic Scenarios. In Proceedings of the 2019 IEEE Intelligent Transportation Systems Conference (ITSC), Auckland, New Zealand, 27–30 October 2019; pp. 3149–3154.
22. Artuñedo, A.; Gonzalez, M.; Villagra, J. Lateral Control for Autonomous Vehicles: A Comparative Evaluation. *Annu. Rev. Control* **2024**, *57*, 100910. [CrossRef]
23. Kim, G.; Park, C.; Jeong, C. Vehicle's Lateral Motion Control Using Dynamic Mode Decomposition Model Predictive Control for Unknown Model. *Int. J. Automot. Technol.* **2024**, *25*, 999–1009. [CrossRef]
24. Spike, N.; Robinette, D.; Bos, J. Cross-Track-Compensated Pure Pursuit Control of an Autonomous Vehicle on Low-Friction Surfaces. *SAE Int. J. Connect. Autom. Veh.* **2021**, *4*, 177–188. [CrossRef]
25. Thrun, S.; Montemerlo, M.; Dahlkamp, H. Stanley: The Robot that Won the DARPA Grand Challenge. *J. Field Robot.* **2006**, *23*, 661–692. [CrossRef]
26. Raffo, G.; Gomes, G.; Rico, J. A Predictive Controller for Autonomous Vehicle Path Tracking. *IEEE Trans. Intell. Transp. Syst.* **2009**, *10*, 92–102. [CrossRef]
27. Lee, A. Performance of Four-Wheel-Steering Vehicles in Lane Change Maneuvers. *SAE Tech. Pap.* **1995**, 161–173. [CrossRef]
28. Mashadi, B.; Ahmadizadeh, P.; Majidi, M. Integrated Robust Controller for Vehicle Path Following. *Multibody Syst. Dyn.* **2015**, *33*, 207–228. [CrossRef]
29. Salehpour, S.; Pourasad, Y.; Taheri, S. Vehicle Path Tracking by Integrated Chassis Control. *J. Cent. South Univ.* **2015**, *22*, 1378–1388. [CrossRef]
30. Lee, K.; Jeon, S.; Kim, H. Optimal Path Tracking Control of Autonomous Vehicle: Adaptive Full-State Linear Quadratic Gaussian (LQG) Control. *IEEE Access* **2019**, *7*, 109120–109133. [CrossRef]
31. Yakub, F.; Mori, Y. Comparative Study of Autonomous Path-Following Vehicle Control via Model Predictive Control and Linear Quadratic Control. *Proc. Inst. Mech. Eng. Part D J. Automob. Eng.* **2015**, *229*, 1695–1714. [CrossRef]
32. Ghandriz, T.; Jacobson, B.; Nilsson, P. Trajectory-Following and Off-Tracking Minimisation of Long Combination Vehicles: A Comparison between Nonlinear and Linear Model Predictive Control. *Veh. Syst. Dyn.* **2024**, *62*, 277–310. [CrossRef]
33. Vaskov, S.; Quirynen, R.; Menner, M. Friction-Adaptive Stochastic Nonlinear Model Predictive Control for Autonomous Vehicles. *Veh. Syst. Dyn.* **2024**, *62*, 347–371. [CrossRef]
34. Goh, J.; Thompson, M.; Dallas, J. Beyond the Stable Handling Limits: Nonlinear Model Predictive Control for Highly Transient Autonomous Drifting. *Veh. Syst. Dyn.* **2024**, *62*, 2590–2613. [CrossRef]
35. Singh, A.S.P.; Nishihara, O. Trajectory Tracking and Integrated Chassis Control for Obstacle Avoidance with Minimum Jerk. *IEEE Trans. Intell. Transp. Syst.* **2022**, *23*, 4625–4641. [CrossRef]
36. Awad, N.; Lasheen, A.; Elnaggar, M. Model Predictive Control with Fuzzy Logic Switching for Path Tracking of Autonomous Vehicles. *ISA Trans.* **2022**, *129*, 193–205. [CrossRef] [PubMed]
37. Borrell, A.; Puig, V.; Sename, O. Fixed-Structure Parameter-Dependent State Feedback Controller: A Scaled Autonomous Vehicle Path-Tracking Application. *Control Eng. Pract.* **2024**, *147*, 105911. [CrossRef]
38. Hashemi, E.; Khajepur, A. Integrated Path-Tracking and Combined-Slip Force Controls of Autonomous Ground Vehicles with Safe Constraints Adaptation. *IEEE Trans. Intell. Veh.* **2024**, *9*, 4265–4274. [CrossRef]
39. Choi, Y.; Park, J. Game-Based Lateral and Longitudinal Coupling Control for Autonomous Vehicle Trajectory Tracking. *IEEE Access* **2021**, *10*, 31723–31731. [CrossRef]
40. Balint, K.; Gergo, A.; Tamas, B. Deep Reinforcement Learning Combined with RRT for Trajectory Tracking of Autonomous Vehicles. *Transp. Res. Procedia* **2024**, *78*, 246–253. [CrossRef]
41. Viscaya, J.A.M.; Gutiérrez, A.I.B.; Gómez, G.G. Design, Construction, and Validation of an Experimental Electric Vehicle with Trajectory Tracking. *Sensors* **2024**, *24*, 2769. [CrossRef]
42. Taghavifar, H.; Mohammadzadeh, A.; Zhang, W. Nonsingleton Gaussian Type-3 Fuzzy System with Fractional Order NTSMC for Path Tracking of Autonomous Cars. *ISA Trans.* **2024**, *146*, 75–86. [CrossRef]
43. Sanchez, A.; Poznyak, A.; Chairez, I. Extremum Seeking Control for the Trajectory Tracking of a Skid Steering Vehicle via Averaged Sub-Gradient Integral Sliding-Mode Theory. *Robot. Auton. Syst.* **2024**, *174*, 104609. [CrossRef]
44. Loyola, J.; Margolis, D. Variable Wheelbase Reference for Vehicle with Active Front and Rear-Wheel Steering. *Veh. Syst. Dyn.* **2022**, *60*, 2758–2774. [CrossRef]
45. Liu, Q.; Gordon, T.; Rahman, S. Model-Free Autonomous Control of Four-Wheel Steering using Artificial Flow Guidance. *Veh. Syst. Dyn.* **2024**, *62*, 1565–1586. [CrossRef]
46. Jeong, Y.; Yim, S. Path Tracking Control with Four-Wheel Independent Steering, Driving and Braking Systems for Autonomous Electric Vehicles. *IEEE Access* **2022**, *10*, 74733–74746. [CrossRef]
47. Lai, F.; Wang, X. Enhancing Autonomous Vehicle Stability through Pre-Emptive Braking Control for Emergency Collision Avoidance. *Appl. Sci.* **2023**, *13*, 13219. [CrossRef]
48. Yim, S. Comparison among Active Front, Front Independent, 4-Wheel and 4-Wheel Independent Steering Systems for Vehicle Stability Control. *Electronics* **2020**, *9*, 798. [CrossRef]
49. Kim, Y.; Ji, Y.; Yoon, S. Control Interface for Next Generation Vehicles: What is the Best Way to Drive Four-Wheel Independent Steering Vehicles? *Int. J. Hum.-Comput. Interact.* **2024**, *40*, 1586–1599. [CrossRef]

50. He, C.; Jiang, W.; Li, J.; Wei, J.; Guo, J.; Zhang, Q. Fuzzy Logic-Based Autonomous Lane Changing Strategy for Intelligent Internet of Vehicles: A Trajectory Planning Approach. *World Electr. Veh. J.* **2024**, *15*, 403. [CrossRef]
51. Alleyne, A. A Comparison of Alternative Obstacle Avoidance Strategies for Vehicle Control. *Veh. Syst. Dyn.* **1997**, *27*, 371–392. [CrossRef]